Mapping the Inside of the Ribosome with an RNA Helical Ruler

Simpson Joseph, Bryn Weiser, Harry F. Noller*

The structure of ribosomal RNA (rRNA) in the ribosome was probed with hydroxyl radicals generated locally from iron(II) tethered to the 5′ ends of anticodon stem-loop analogs (ASLs) of transfer RNA. The ASLs, ranging in length from 4 to 33 base pairs, bound to the ribosome in a messenger RNA–dependent manner and directed cleavage to specific regions of the 16S, 23S, and 5S rRNA chains. The positions and intensities of cleavage depended on whether the ASLs were bound to the ribosomal A or P site, and on the lengths of their stems. These data predict the three-dimensional locations of the rRNA targets relative to the positions of A- and P- site transfer RNAs inside the ribosome.

Translation, the process of protein synthesis, includes physical and chemical interactions between the mRNA-programmed ribosome and its substrate, transfer RNA (tRNA). Little is known about the molecular mechanics of translation, which must involve dynamic interactions between tRNA and the interior surface of the ribosome, in the cavity between its two subunits. The small (30S) ribosomal subunit, which contains 16S rRNA and 21 proteins, interacts with the anticodon ends of the L-shaped tRNAs, as well as with messenger RNA (mRNA), and directs codon-anticodon interaction. The large (50S) subunit, which contains 23S and 5S rRNAs and more than 30 proteins, interacts with the acceptor ends of the tRNAs and contains the catalytic site of peptidyl transferase. An important step toward understanding the mechanism of translation is, therefore, to map the molecular features of the subunit interface, particularly those surrounding the tRNAs. The interface surface is believed to be RNA-rich (*1*); indeed, elements of both 16S and 23S rRNA have been located at the subunit interface (*2–4*).

A growing body of evidence points to a direct role for ribosomal RNA (rRNA) in the interaction between the tRNA and ribosome. Cross-linking (*5–11*), chemical footprinting (*12, 13*), modification-interference experiments (*14*), and in vitro genetics (*15*) have identified specific features of 16S and 23S rRNA as elements of the structural environment of tRNA in the ribosome. We recently made use of a method, involving directed hydroxyl-radical probing by Fe(II) tethered to the 5′-end of tRNA via the linker [1-(*p*-bromoacetamidobenzyl)-EDTA] (BABE) (*16*), to map several regions of 23S rRNA that are proximal to the acceptor end of tRNA in the ribosomal A, P, and E sites (*17*). Hydroxyl radicals are believed to attack the ribose moiety of RNA in a reaction that leads to scission of the sugar-phosphate backbone (*18*). We now describe a variation of this approach to explore systematically the inside of the ribosome with an RNA "helical ruler." In previous studies by Eckstein and co-workers, RNA helix length was used to calibrate molecular distances for fluorescence energy transfer experiments (*19*). We use a series of tRNA anticodon stem-loop analogs (ASLs) of increasing lengths, from 4 to 33 base pairs (bp), extending by increments of 2 to 3 bp (Fig. 1) (*20*). These in vitro–transcribed ASLs, with Fe(II) coupled to their 5′ phosphorothioate ends by the BABE linker, were bound specifically to the 70S ribosome in the 30S P or A site. Hydroxyl radicals were then generated locally to probe the rRNA surrounding the tethered Fe(II). The strength of cleavage at the rRNA target sites, as a function of ASL length, constrains the positions of these rRNA elements in three-dimensional space around the bound tRNAs.

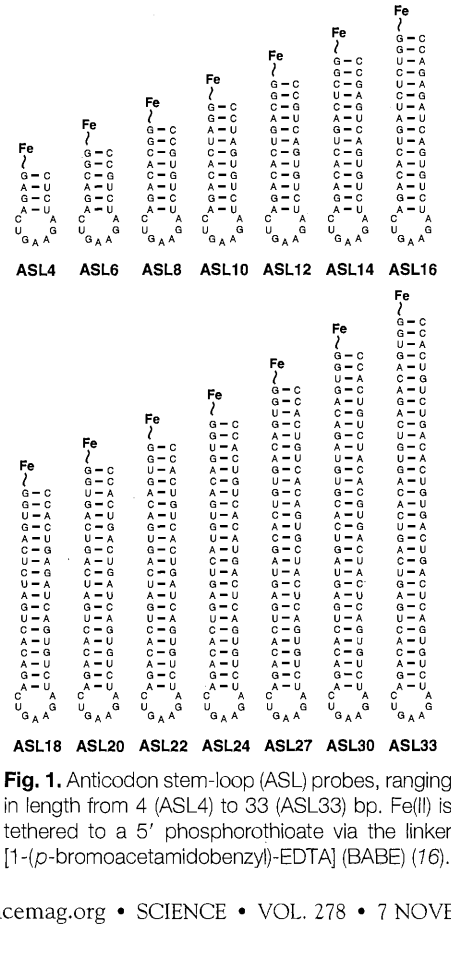

Fig. 1. Anticodon stem-loop (ASL) probes, ranging in length from 4 (ASL4) to 33 (ASL33) bp. Fe(II) is tethered to a 5′ phosphorothioate via the linker [1-(*p*-bromoacetamidobenzyl)-EDTA] (BABE) (*16*).

Binding the ASLs to the ribosome. The ASLs, based on the yeast $tRNA^{Phe}$ sequence, were bound specifically to the A or P site of ribosomes programmed with mRNA for phage T4 gene 32 (Fig. 2). Footprinting experiments verified the positions of the ASLs to the A and P sites; all of the observed ASL-dependent cleavages were mRNA-dependent and could be competed away by excess full-length $tRNA^{Phe}$ (*21*). These data indicate that the ASLs bind correctly to their ribosomal binding sites.

Figures 3 and 4 show autoradiographs of primer extension analyses of rRNA extracted from ribosomes subjected to directed cleavage. The gel lanes correspond to complexes formed with ASLs of increasing stem length, from left to right, beginning with the 15-nucleotide (nt), 4-bp ASL4. Directed cleavages are detected as bands that appear in one or more experimental lanes but are missing in the control lanes.

Probing from the P site. When ASLs were bound to the small-subunit P site (Fig.

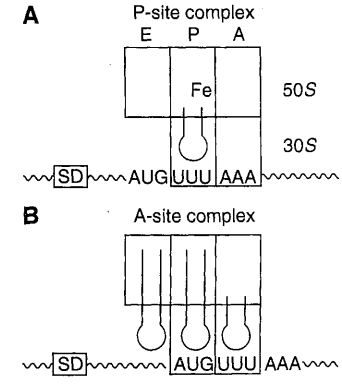

Fig. 2. Gene 32 mRNA-directed binding of ASLs to the ribosomal P or A sites. (**A**) ASLs are positioned in the high-affinity P site by their cognate UUU codon in the absence of $tRNA_f^{Met}$. (**B**) Binding of $tRNA_f^{Met}$ to the AUG initiator codon in the P (and E) site directs binding of ASLs to the UUU codon in the A site. SD, Shine-Dalgarno sequence.

The authors are at the Center for Molecular Biology of RNA, Sinsheimer Laboratories, University of California, Santa Cruz, CA 95064, USA.

*To whom correspondence should be addressed. E-mail: harry@nuvolari.ucsc.edu

2A), hydroxyl radicals generated from their 5′-tethered Fe(II) moieties caused cleavage at specific positions of all three ribosomal RNAs, as shown in Fig. 3 and summarized in Fig. 5. Different rRNA targets are cleaved with varying efficiencies, reflecting their proximities to the Fe(II) probe. There is a marked dependency of the strength of cleavage of each target on the helix length of the ASL probes. For a standard RNA A-form helix, each 2-bp increment corresponds to a translation by about 6 Å, and rotation of about 65°, with respect to the helical axis, resulting in a displacement of about 12 Å between successive tethering positions (or about 18 Å for 3-bp increments). Thus, both the strength of cleavage and the length of ASL provide information about the rRNA target position. Several of the ASL-dependent cleavages in 16S rRNA are in regions that have been implicated in P-site binding in earlier experiments. These include bases in the 690 and 790 hairpin loops, and in the internal loop around position 1338 (Fig. 3, A, B, and E). In addition, we observe cleavages around positions 1227 and 1299 (Fig. 3, C and D). The 790, 1227, and 1338 regions are hit most strongly from the shorter-length helical probes (ASLs 4 to 6), whereas cleavage of the 695 and 1299 regions is optimal for ASLs of length 10 and 14, respectively (Fig. 3, A and D). The 785 region, which is cleaved less strongly than the 790 region, has an optimum around ASL10 (Fig. 3B), even though it is only a few nucleotides away from position 790. These data provide clues to the geometry of this part of 16S rRNA, relative to P-site tRNA, as discussed below.

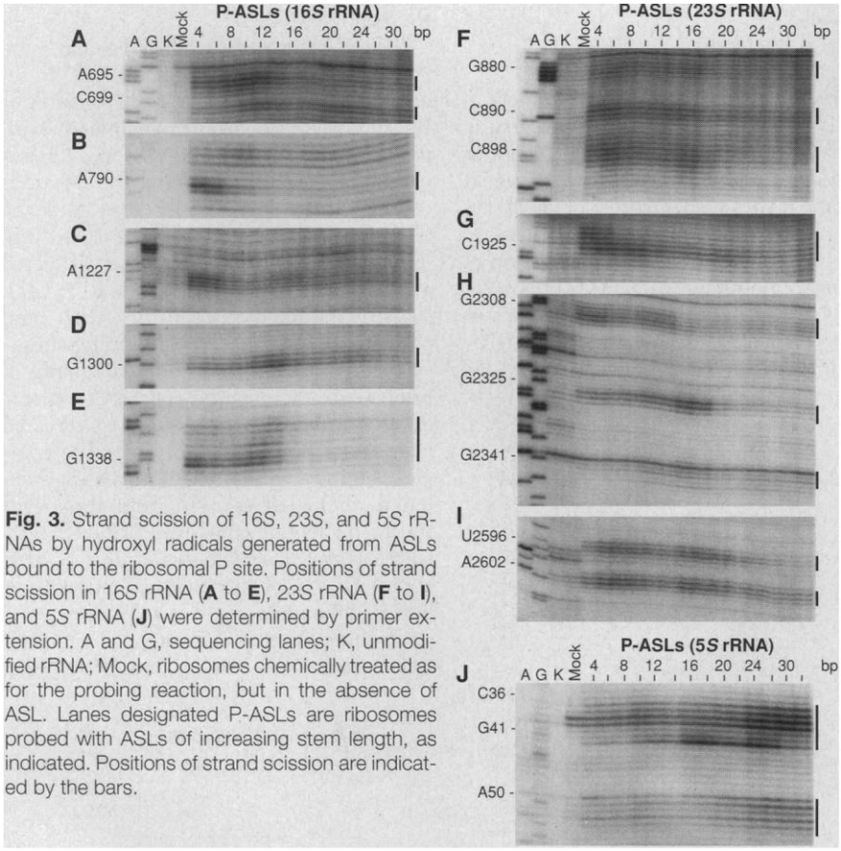

Fig. 3. Strand scission of 16S, 23S, and 5S rRNAs by hydroxyl radicals generated from ASLs bound to the ribosomal P site. Positions of strand scission in 16S rRNA (**A** to **E**), 23S rRNA (**F** to **I**), and 5S rRNA (**J**) were determined by primer extension. A and G, sequencing lanes; K, unmodified rRNA; Mock, ribosomes chemically treated as for the probing reaction, but in the absence of ASL. Lanes designated P-ASLs are ribosomes probed with ASLs of increasing stem length, as indicated. Positions of strand scission are indicated by the bars.

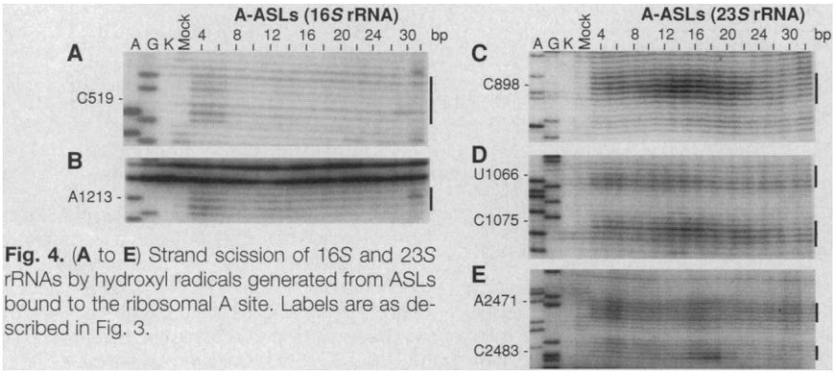

Fig. 4. (**A** to **E**) Strand scission of 16S and 23S rRNAs by hydroxyl radicals generated from ASLs bound to the ribosomal A site. Labels are as described in Fig. 3.

Although the shorter ASLs (and possibly all of them) are believed to interact in the P site exclusively with the small subunit, we also observe ASL-dependent cleavage of several sites in 23S rRNA and 5S rRNA, which are components of the large subunit. While these tend to be cleaved by ASLs of longer stem length, several notable targets in 23S rRNA are also cleaved by relatively short ASLs, indicating close proximity of their anticodon stems to specific regions of 23S rRNA (Fig. 3, F to I). In 23S rRNA, the most prominent cleavages occur around nucleotide positions 880, 890, 900, 1925, 2325, 2595, and 2600.

Two regions of 5S rRNA, around positions 35 to 41 and 49 to 53, are also cleaved by P-site ASLs (Fig. 3J). The most efficient cleavage of 5S rRNA targets is from very long ASLs—from ASL16 to 33—indicating that these are the most remote targets from the decoding site that we observe for any region of rRNA. Maximum cleavage of positions 35 to 38 and 49 to 53 is seen with ASLs of 30 and 24 bp, respectively; these probes extend well beyond the envelope of the crystal structure of tRNA (see below).

A second maximum can often be seen at ASL lengths differing by 10 to 12 bp from the optimal cleavage length. An example is cleavage of position 900 of 23S rRNA by P-site ASLs. Strongest cleavage is observed with ASL6, but a second maximum, around ASL16, and a weaker one around ASL24, are also apparent. Because the helical repeat for A-form RNA is about 11 bp (*22*), the phased repeat of cleavage intensity indicates that the face of the probe helix defined by the 5′ positions of the ASLs at the two maxima is nearest to the rRNA target. For P-site targets, a similar variance in the distribution of cleavage bands at both maxima is observed. This provides evidence that the ASLs are bound rigidly in the P site; otherwise, a broader distribution of cleavages would be expected for the longer ASLs. In contrast, the A-site cleavage patterns tend to be broader and more diffuse for longer ASLs (for example, C898 and C1075 regions) (Fig. 4, C and D), suggesting that A-site ASLs have greater freedom of movement.

Probing from the A site. Cleavage patterns observed for the A-site ASLs (Fig. 4) were distinct from those observed for the P site. None of the P-site target regions were hit from A-site ASLs, with the exception of the 900 region of 23S rRNA, which, how-

ever, showed a markedly different dependence on ASL length when probed from the A site (Fig. 4C); nor was any cleavage of 5S rRNA observed. These findings provide additional evidence for high specificity of A- and P-site binding of the ASLs.

Cleavage of 16S rRNA from the A site was comparatively weak and was observed only for very short ASLs (Fig. 4, A and B). The 514 to 520 region on the 5′ side of the 530 loop, and nt 1210 to 1214 in the 3′ major domain, were accessible to ASLs 4 and 6. The low relative intensity of the bands suggests that both regions of 16S rRNA are near the outer limits of the range of the probes, whereas several targets in 23S rRNA appear to be in closer proximity. The accessibility of the 900 region in domain II of 23S rRNA to both A- and P-site ASLs (Figs. 3F and 4C) indicates that it must be positioned on the subunit interface surface of the 50S subunit in a way that straddles both the A and P sites. Cleavage of the 1066 and 1075 regions of domain II of 23S rRNA, which is maximal from ASLs 14 to 16 (Fig. 4D), targets one of the two known sites of interaction of elongation factor EF-G with 23S rRNA (*23*, *24*). The 2470 to 2485 stem in domain V of 23S rRNA is also hit from A-site ASLs, albeit more weakly (Fig. 4E).

Mapping the three-dimensional locations of rRNA targets. These cleavage data provide information about the locations of the rRNA targets with respect to the positions of ribosome-bound tRNAs. An important link is the relation between ASL structure and the geometry of the corresponding tRNAs. We can infer the locations of the Fe(II) tethering sites in the different ASLs relative to the positions of A- and P-site tRNAs by superimposing their respective anticodon loops (Fig. 6) (*25*). We assume that the structures of the tRNAs in the ribosome are similar to their crystal structures, and that the ASLs bind to the ribosome following the paths of the anticodon stem-loops of the corresponding tRNAs. At helix lengths beyond ASL20, the probe helix extends beyond the envelope of the tRNA structure at its elbow region, near the T loop. It is remarkable that all of the ASL analogs, including ASL33, which extends some 40 Å beyond the boundaries of the tRNA structure, appear to bind normally to 70S ribosomes in a mRNA-dependent manner to both A and P sites and give the correct 16S rRNA footprints in all cases.

On the basis of the superimposition shown in Fig. 6, together with the dependence of cleavage intensity as a function of ASL length, we can triangulate the approximate spatial positions of the rRNA targets relative to the A- and P-site tRNAs, using the cleavage intensity data for a given target from ASLs of different lengths. The intensity of cleavage depends on the proximity of the rRNA target to the probe position due to the limited range of diffusion of hydroxyl radicals. The dependence of cleavage intensity on distance was calibrated in two independent ways that were in generally good agreement with each other (*26*) and with published estimates (*27*). We generated spheres or shells corresponding to these ranges, centered on the tethering positions, and estimated the position of a given target to be within a cloud corresponding to the overlapping spatial volume in common to the different spheres and shells (after subtracting the volume of the ASL helix itself). Some examples of these computations, in which the target clouds are displayed in context of the modeled tRNA pair, are shown in Fig. 7. Targets that are hit strongly, such as positions 790 of 16S rRNA (Fig. 7A) and 1921 of 23S rRNA (Fig. 7C), have smaller clouds, and so their possible spatial positions are constrained to a smaller volume. Conversely, the allowed locations of more weakly cleaved sites, such as position 2471 of 23S rRNA (Fig. 7D), are spread over a relatively large volume. Comparison of the cloud volumes in Fig. 7 indicates that the A-site clouds are more diffuse than the P-site clouds, consistent with the

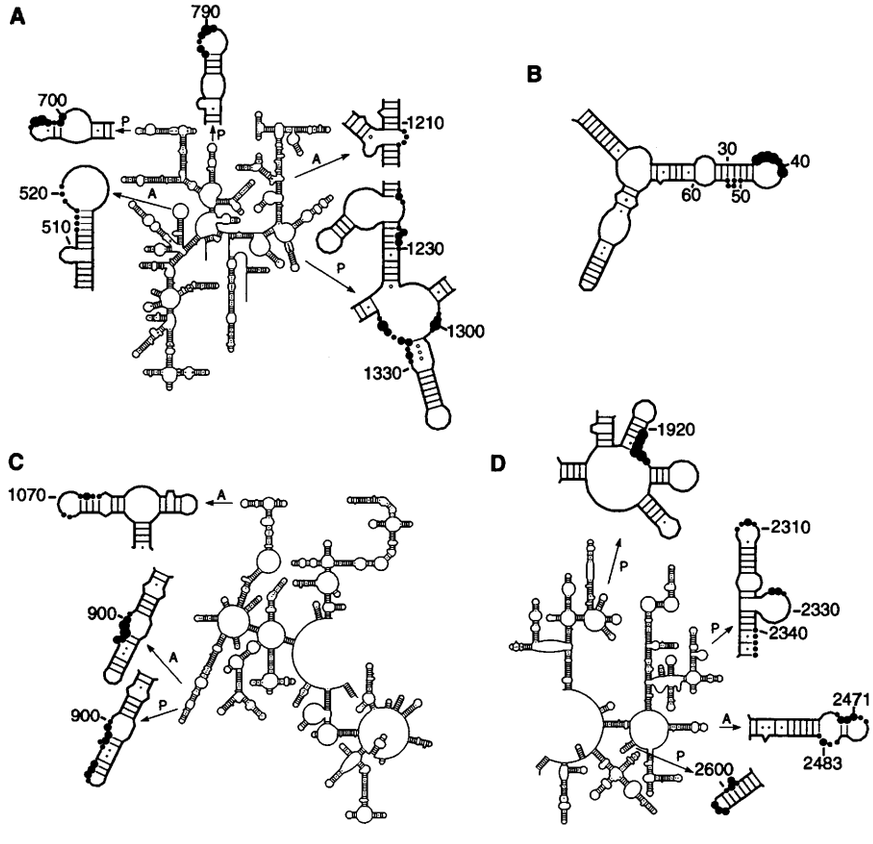

Fig. 5. Locations of rRNA targets in (**A**) 16S rRNA, (**B**) 5S rRNA, (**C**) 5′-half of 23S rRNA, and (**D**) 3′-half of 23S rRNA. Sizes of the filled circles are proportional to strengths of cleavages. P and A, scissions generated from ASLs bound to the P or A site, respectively.

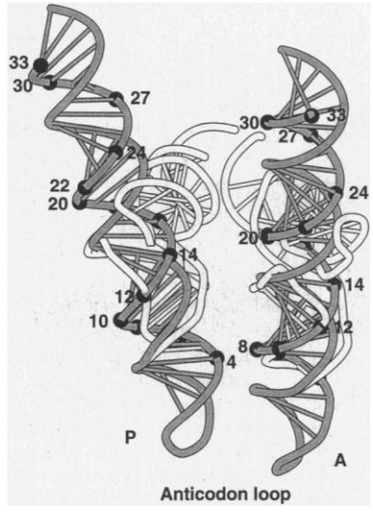

Fig. 6. Locations of ASL 5′ tethering positions relative to the modeled positions of P- and A-site tRNAs. Positions of 5′ phosphates (black spheres) of ASLs 4-33 are indicated on ASL33 (shaded). The two ASLs were docked on the tRNA structures by superimposition of their respective 4-bp anticodon stem-loops (*25*).

possibility that the ASLs have greater freedom of motion in the A site, as discussed above. This could be due to the weaker affinity of the A site for tRNA, or to the necessity for the ribosome to accommodate significant movement of tRNA from the A/T (EF-Tu–bound) state to the A/A state while maintaining codon-anticodon interaction (*13*), or to both of these factors.

P-site ASLs target four main regions of 16*S* rRNA, around positions 695, 790, 1300, and 1338 (Fig. 5A). Bases in all three regions were implicated as components of the 30*S* subunit P site in earlier chemical footprinting, modification interference, and cross-linking studies (*8*, *12*, *14*). Their predicted locations cluster around the anticodon arm of peptidyl-tRNA, consistent with the current view that the anticodon stem-loop of P-site tRNA is bound in the "cleft" of the small subunit (*28*–*31*). Moreover, the 690 and 790 loops have been located on the "platform" of the small subunit, which forms the outer boundary of the cleft, whereas the 1338 internal loop has been located in the "head" of the subunit, lining the inside of the cleft (*29*, *30*). It can be inferred that the platform lies to the left of the P-site tRNA anticodon arm, and that the head of the subunit is on the near side, as viewed in Fig. 7.

The 790 loop has also strongly been implicated in interactions with the large subunit (*2*, *4*, *32*); its predicted location on the opposite side of the anticodon stem (Fig. 7A) faces the surface of the large subunit where the main "bridge" between the two subunits has been identified by electron microscopy (EM) reconstruction studies (*33*, *34*). One of the main elements of 23*S* rRNA known to interact with the 30*S* subunit is the 1920 region of domain IV (*35*), which is among the targets hit by P-site ASLs in the range of ASL4 to 10 (Fig. 3G). The 1920 region is protected from chemical probes by subunit association (*4*, *36*) and has been cross-linked to elements of the 16*S* rRNA decoding site (*3*). The predicted location of position 1921 (Fig. 7C) is centered on the 50*S* face of the anticodon loop, very close to the position of the 790 loop (Fig. 7A). These two RNA elements are therefore likely to be main structural features of the observed intersubunit bridge.

Another target of P-site ASLs is the bulged stem-loop around position 2600 of 23*S* rRNA (Fig. 5D) that has been placed near the peptidyl transferase center of the large subunit (*13*). This feature of rRNA, which appears to undergo a functionally significant conformational transition, was hit weakly by hydroxyl radicals generated from Fe(II) tethered to the 5′ end of full-length tRNA (*17*). In this study, it is cleaved somewhat more strongly from medium-length ASL probes. The predicted locations of nt 2596 and 2602 place the 2600 stem to the lower left of, and oriented ap-

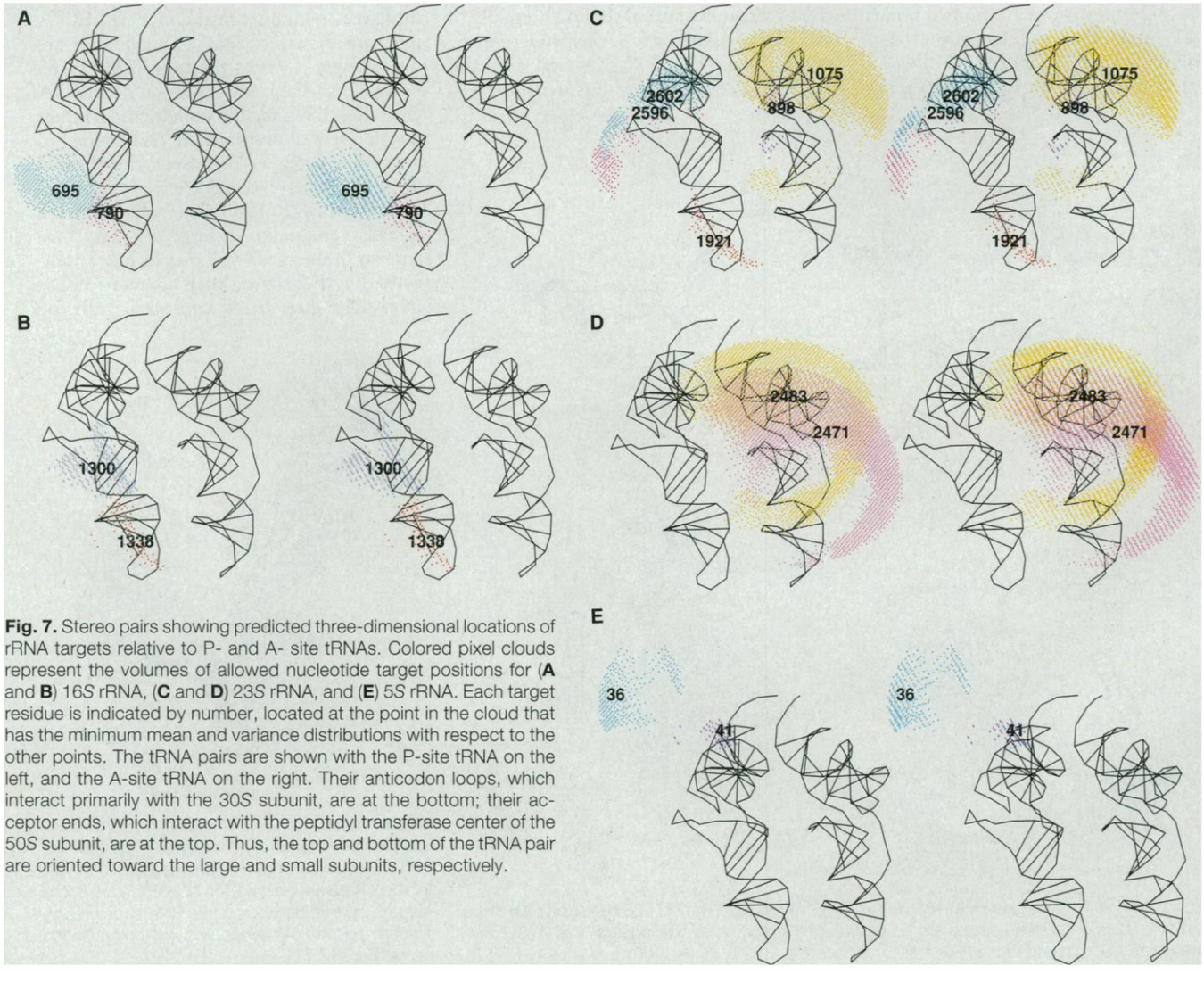

Fig. 7. Stereo pairs showing predicted three-dimensional locations of rRNA targets relative to P- and A- site tRNAs. Colored pixel clouds represent the volumes of allowed nucleotide target positions for (**A** and **B**) 16*S* rRNA, (**C** and **D**) 23*S* rRNA, and (**E**) 5*S* rRNA. Each target residue is indicated by number, located at the point in the cloud that has the minimum mean and variance distributions with respect to the other points. The tRNA pairs are shown with the P-site tRNA on the left, and the A-site tRNA on the right. Their anticodon loops, which interact primarily with the 30*S* subunit, are at the bottom; their acceptor ends, which interact with the peptidyl transferase center of the 50*S* subunit, are at the top. Thus, the top and bottom of the tRNA pair are oriented toward the large and small subunits, respectively.

proximately parallel to, the P-site acceptor arm, with the loop pointing toward the small subunit. This arrangement places the central loop of domain V near the acceptor end of P-site tRNA, in agreement with a large body of evidence (*35*).

The stem protruding from the right-hand side of the central loop of domain V (positions 2455 to 2496) is targeted from A-site ASLs (Fig. 5D). Although this stem is only approximately constrained by the relatively weak cleavages, its likely position is to the lower right of the acceptor stem of A-site tRNA (Fig. 7D). The 2471 region has a strong maximum at ASL6 and a weaker one at ASL16, whereas the nearby 2483 region shows the opposite behavior (Fig. 4E), providing clues to the local orientation of this stem. Again, these findings are consistent with placement of the central loop of domain V in the general vicinity of the tRNA acceptor ends.

Two sites of functional interest in domain II of 23S rRNA are cleaved by A-site ASLs. The region around 1060 to 1100 interacts with elongation factor EF-G (*23*, *24*) and with the antibiotic thiostrepton, an inhibitor of translocation (*37*). This element of 23S rRNA is located to the right of the acceptor arm of A-site tRNA (Fig. 7C), a position that is consistent with current knowledge about the binding site of EF-G. A second antibiotic target site in domain II of 23S rRNA is the 900 stem, the only rRNA target that is cleaved by ASL probes from both the A and P sites. The 900 region is footprinted by viomycin, another inhibitor of translocation (*38*). Its predicted location, under the elbow of A-site tRNA, near that of position 1075 (Fig. 7C), suggests that viomycin could act by physically blocking movement of tRNA from the A to the P site. The nearby 890 loop of 23S rRNA has been cross-linked to position 20:1 on the left side of the elbow of A-site tRNA, and more weakly from positions 8 and 47, which lie on the opposite face of the tRNA (*9*, *10*).

A-site ASLs cleave 16S rRNA only weakly, around positions 520 and 1215 (Fig. 5A). We estimate these targets to lie toward the near right-hand side of the A-site anticodon stem, although their positions are poorly constrained because of the weakness of their respective cleavages. Similarly, the relatively weak P-site cleavages between positions 2300 and 2340 in domain V of 23S rRNA place these features within about 35 Å from the left-hand side of the P-site tRNA elbow, toward the large subunit, in good agreement with the observed cross-links to this region from the elbow of P-site tRNA (*9*, *10*). The weakness of many of the A-site cleavages could also be due, in part, to possible greater freedom of motion of the ASLs in the A site, as discussed above.

The predicted location of 5S rRNA (Fig. 7E) is above and to the left of the elbow of P-site tRNA, in reasonable agreement with its placement by previous studies in the central protuberance of the 50S subunit and with the roughly constrained location of the 2300 to 2340 region, to which 5S rRNA has been cross-linked (*39*).

Some targets are conspicuous by their absence. These include bases G926, ^{2m}G966, and G1401 of 16S rRNA, which are believed to interact with the anticodon stem-loop of P-site tRNA (*12*, *14*), and the 1492 to 1493 region of 16S rRNA, which is protected by binding of the A-site tRNA anticodon stem-loop (*12*). We suggest that these elements of rRNA, perhaps because of direct involvement in codon-anticodon interactions, may be inaccessible to attack by free radicals when the tRNA binding sites are occupied. This interpretation is consistent with the previous finding that the anticodon stem-loop of tRNA is itself shielded from hydroxyl radicals when bound to the 30S subunit (*40*).

No rRNA targets map to the space between the A- and P-site tRNAs, which provides for unobstructed movement of tRNA between the A and P sites. Nor are any rRNA elements found in the region where the extra stem of type II tRNAs would protrude (*41*). However, there is at least one location where elements of rRNA may pose a potential barrier to tRNA movement. The predicted positions of the 690 and 790 stem-loop structures of 16S rRNA (Fig. 7A) (and possibly the 2600 stem of 23S rRNA) (Fig. 7C) would appear to block leftward movement of the deacylated tRNA as it exits the small subunit. One or more of these elements would have to move out of the path of the exiting tRNA, or its path would have to be orthogonal to that of A-to-P movement. Recent EM reconstructions suggest a much larger displacement of the anticodon stem during P to E translocation than for A to P movement. Because binding to the 30S subunit P site is much stronger than to its A site (*42*), the main energy barrier for the step of translocation on the small subunit (the EF-G–catalyzed step) may be disruption of P-site binding. This could be accomplished by transient rearrangement of the structure of the cleft of the small subunit, which could also be coupled to large-scale movement of the exiting tRNA.

Previous studies have shown that the two functionally important extremities of tRNA, the anticodon stem-loop and acceptor ends, are in an rRNA-rich environment in the ribosome (*35*). Our present findings support this view and provide a detailed catalog of the internal solvent-accessible features of rRNA that are positioned near the A- and P-site tRNAs and elsewhere in the intraribosomal cavity. Because of the low sequence and structural specificity of hydroxyl radicals for their RNA targets (*18*), this catalog should be a fairly comprehensive one, which can serve as a useful guide for future studies on RNA function and architecture in the ribosome.

REFERENCES AND NOTES

1. W. Kühlbrandt and P. N. T. Unwin, *J. Mol. Biol.* **156**, 431 (1982); M. M. Yusupov and A. S. Spirin, *FEBS Lett.* **197**, 229 (1986); J. Frank, P. Penczek, R. Grassucci, S. Srivastava, *J. Cell. Biol.* **115**, 597 (1991); W. D. Picking, O. W. Odom, B. Hardesty, *Biochemistry* **31**, 12565 (1992).
2. N. M. Chapman and H. F. Noller, *J. Mol. Biol.* **109**, 131 (1977); W. Herr, N. M. Chapman, H. F. Noller, *ibid.* **130**, 433 (1979); S. K. Vassilenko, P. Carbon, J.-P. Ebel, C. Ehresmann, *ibid.* **152**, 699 (1981).
3. P. Mitchell, M. Oßwald, R. Brimacombe, *Biochemistry* **31**, 3004 (1992).
4. C. Merryman, D. Moazed, J. McWhirter, H. F. Noller, unpublished data.
5. J. B. Prince, B. H. Taylor, D. L. Thurlow, J. Ofengand, R. A. Zimmermann, *Proc. Natl. Acad. Sci. U.S.A.* **79**, 5450 (1982).
6. A. Barta, G. Steiner, J. Brosius, H. F. Noller, E. Kuechler, *ibid.* **81**, 3607 (1984).
7. J. Wower, S. S. Hixson, R. A. Zimmermann, *ibid.* **86**, 5232 (1989).
8. T. Döring, P. Mitchell, M. Oßwald, D. Bochkariov, R. Brimacombe, *EMBO J.* **13**, 2677 (1994).
9. M. Oßwald, T. Döring, R. Brimacombe, *Nucleic Acids Res.* **23**, 4635 (1995).
10. A. J. Rinke, N. Junke, M. Oßwald, R. Brimacombe, *RNA* **1**, 1018 (1995).
11. P. Mitchell, K. Stade, M. Oßwald, R. Brimacombe, *Nucleic Acids Res.* **21**, 887 (1993).
12. D. Moazed and H. F. Noller, *Cell* **47**, 985 (1986); *J. Mol. Biol.* **211**, 135 (1990).
13. ———, *Cell* **57**, 585 (1989); *Proc. Natl. Acad. Sci. U.S.A.* **88**, 3725 (1991).
14. U. von Ahsen and H. F. Noller, *Science* **267**, 234 (1995).
15. R. R. Samaha, R. Green, H. F. Noller, *Nature* **377**, 309 (1995).
16. L. H. DeRiemer, C. F. Meares, D. A. Goodwin, C. J. Diamanti, *J. Labelled Compd. Radiopharm.* **18**, 1517 (1981); T. M. Rana and C. F. Meares, *J. Am. Chem. Soc.* **112**, 2457 (1990).
17. S. Joseph and H. F. Noller, *EMBO J.* **15**, 910 (1996).
18. R. P. Hertzberg and P. B. Dervan, *Biochemistry* **23**, 3934 (1984); J. A. Latham and T. R. Cech, *Science* **245**, 276 (1989); D. W. Celander and T. R. Cech, *Biochemistry* **29**, 1355 (1990); W. K. Pogozelski, T. J. McNeese, T. D. Tullius, *J. Am. Chem. Soc.* **117**, 6428 (1995).
19. T. Tuschl, C. Gohlke, T. M. Jovin, E. Westhof, F. Eckstein, *Science* **266**, 785 (1994).
20. ASLs were synthesized by in vitro transcription with T7 RNA polymerase from synthetic oligodeoxynucleotide templates. For 5′-derivatization with BABE, a 5′-phosphorothioate was introduced by transcription in the presence of 5′-guanosine-α-phosphorothioate (GMPS) essentially as described (*17*) and in the presence of low concentrations of [α-^{32}P]cytidine 5′-triphosphate as tracer. ASL sequences were confirmed by complete digestion with ribonuclease (RNase) T1 and analysis by high-voltage paper electrophoresis. Their predicted secondary structures were confirmed by partial RNase digestion. Derivatization with Fe(II)BABE and purification was essentially as described (*17*). Construction of P-site complex: Ribosomes were preincubated at 42°C for 10 min, followed by addition of gene 32 mRNA and incubated at 37°C for 6 min. BABE-modified ASLs (50 pmol) were bound to the ribosomal P-site by incubation with 10 pmol of tight couple 70S ribosomes in the presence of 2.5 μg of gene 32 mRNA in 25 μl of 80 mM potassium cacodylate (pH

7.2), 20 mM Mg acetate, 150 mM NH_4Cl for 20 min at 37°C and for 20 min on ice. Construction of the A-site complex was as described for the P-site complex except that after addition of gene 32 mRNA, 70S ribosomes were first incubated with 50 pmol of *E. coli* $tRNA_f^{Met}$ for 10 min at 37°C, followed by addition of 150 pmol of 5′-Fe-BABE-ASL, then incubation for 20 min at 37°C and 20 min on ice. Hydroxyl radical strand scission was initiated as described (*17*). Extraction of rRNAs, primer extension, and gel electrophoresis were carried out as described (*43*). All of the observed Fe-BABE–dependent strand scissions were observed in at least three independent experiments and were quantified by PhosphorImager analysis (Molecular Dynamics).

21. S. Joseph and H. F. Noller, unpublished data.
22. S. Arnott, D. W. L. Hukins, S. D. Dover, *Biochem. Biophys. Res. Commun.* **48**, 1392 (1972).
23. S. Sköld, *Nucleic Acids Res.* **11**, 4923 (1983).
24. D. Moazed, J. M. Robertson, H. F. Noller, *Nature* **334**, 362 (1988).
25. The anticodons of two $tRNA^{Phe}$ molecules were base-paired to adjacent codons on a poly(U) mRNA by least-squares fitting to standard A-form helical geometry (*22*). Torsion angles at the junction of the A and P codons were then adjusted until the base-base distances between the A and P tRNAs converged on the values obtained by fluorescence resonance energy transfer (*44*). Independently, they were adjusted to satisfy constraints from hydroxyl-radical probing of A-site tRNA by P-site ASLs, and vice versa (*21*). Both sets of experimental constraints were satisfied well by the arrangement shown in Fig. 6, in which the resulting angle between the planes of the two tRNAs is about 60°. This arrangement is very similar to that originally predicted by Sundaralingam *et al.* (*45*). The structure of ASL33, modeled from the anticodon stem-loop of $tRNA^{Phe}$, extended to 33 bp by standard RNA A helical geometry (*22*), was then docked on each tRNA by least-squares superimposition of ASL4 on nt 28 to 42 of $tRNA^{Phe}$. The predicted locations of the rRNA targets relative to the two tRNAs are independent of the arrangement of the tRNAs; the A- and P-site clouds are, in effect, attached to their respective tRNAs and will simply move along with them.
26. Strong cleavages were defined as those that give rise to gel bands whose intensities are at least two-fold as strong as those of the nearby dideoxy sequencing bands; medium-strength cleavages, as those whose intensities are similar; and weak cleavages, as those whose intensities are half of or less than those of the sequencing bands. Target distances were calibrated in two independent ways. In one case, RNA-RNA duplexes were formed, in which the 5′ end of one strand was derivatized with the Fe(II) probe, and cleavage of the opposite strand was monitored by primer extension. The other approach is an internal calibration inherent in the ASL cleavage data themselves; a lower limit of the probing range for a strong hit at a given target site is half the distance between the two most widely separated ASL tethering sites from which strong cleavage is observed. For example, the maximum separation observed between probe positions for two strong cleavages at the same target is position 1924 by ASL6 and ASL10 (Fig. 3G), corresponding to a distance of about 20 Å between the corresponding ASL phosphate positions. The distance to the target can be estimated as half this distance (10 Å) plus or minus the length of the tether arm (12 Å). This gives a distance range of 0 to 22 Å between the tethering position and target position for strong cleavages. By similar reasoning, we estimate medium-strength cleavages to indicate a range of 12 to 36 Å, and weak cleavages, a range of 20 to 44 Å. The data obtained by means of the duplex method fall into these overlapping ranges, providing independent validation of the values derived from internal calibration. These values are also in good agreement with those reported in previous studies (*27*).
27. G. B. Dreyer and P. B. Dervan, *Proc. Natl. Acad. Sci. U.S.A.* **82**, 968 (1985); H. E. Moser and P. B. Dervan, *Science* **238**, 645 (1987); T. D. Tullius, *Free Radic. Res. Commun.* **2**, 521 (1991); H. Han and P. B. Dervan, *Proc. Natl. Acad. Sci. U.S.A.* **91**, 4955 (1994).
28. P. Gornicki, K. Nurse, W. Hellmann, M. Boublik, J. Ofengand, *J. Biol. Chem.* **259**, 10493 (1984); T. Wagenknecht, J. Frank, M. Boublik, K. Nurse, J. Ofengand, *J. Mol. Biol.* **203**, 753 (1988).
29. S. Stern, B. Weiser, H. F. Noller, *J. Mol. Biol.* **204**, 447 (1988); R. Brimacombe, J. Atmadja, W. Stiege, D. Schuler, *ibid.* **199**, 115 (1988).
30. D. L. Fink, R. O. Chen, H. F. Noller, R. B. Altman, *RNA* **2**, 851 (1996).
31. H. Stark *et al.*, *Cell* **88**, 19 (1997).
32. M. Santer *et al.*, *Proc. Natl. Acad. Sci. U.S.A.* **87**, 3700 (1990); W. E. Tapprich, D. J. Goss, A. E. Dahlberg, *ibid.* **86**, 4927 (1989).
33. J. Frank *et al.*, *Nature* **376**, 441 (1995).
34. H. Stark *et al.*, *Structure* **3**, 815 (1995).
35. H. F. Noller, *Annu. Rev. Biochem.* **60**, 191 (1991); R. Green and H. F. Noller, *ibid.* **66**, 679 (1997).
36. I. Leviev, S. Levieva, R. A. Garrett, *Nucleic Acids Res.* **23**, 1512 (1995).
37. J. Thompson, F. Schmidt, E. Cundliffe, *J. Biol. Chem.* **257**, 7915 (1982).
38. D. Moazed and H. F. Noller, *Biochimie* **69**, 879 (1987).
39. M. Oßwald, B. Greuer, R. Brimacombe, *Nucleic Acids Res.* **18**, 6755 (1990).
40. A. Hüttenhofer and H. F. Noller, *Proc. Natl. Acad. Sci. U.S.A.* **89**, 7851 (1992).
41. V. Biou, A. Yaremchuk, M. Tukalo, S. Cusack, *Science* **263**, 1404 (1994).
42. S. V. Kirillov, V. I. Makhno, Y. P. Semenkov, *Nucleic Acids Res.* **8**, 183 (1980).
43. S. Stern, D. Moazed, H. F. Noller, *Methods Enzymol.* **164**, 481 (1988).
44. A. E. Johnson, H. J. Adkins, E. A. Matthews, C. R. Cantor, *J. Mol. Biol.* **156**, 113 (1982); H. Paulsen, J. M. Robertson, W. Wintermeyer, *ibid.* **167**, 411 (1983).
45. M. Sundaralingam, T. Brennan, N. Yathindra, T. Ichikawa, in *Structure and Conformation of Nucleic Acids and Protein–Nucleic Acid Interactions*, M. Sundaralingam and S. T. Rao, Eds. (University Park, Baltimore, MD, 1975), pp. 101–115.
46. We thank C. R. Woese for suggesting the internal calibration strategy; D. P. Greiner, J. Moran, and C. F. Meares for helping with synthesis of BABE and for providing samples of BABE used in early experiments; members of the Puglisi lab for providing T7 RNA polymerase; M. I. Recht for help with EXCEL; K. Lieberman and R. Green for discussions; and J. Cate, G. Culver, L. Newcomb, R. Green, K. Wilson, K. Lieberman, and L. Holmberg for review of the manuscript. Supported by grant GM-17129 from the NIH and from a grant to the Center for Molecular Biology of RNA from the Lucille P. Markey Charitable Trust.

19 March 1997; accepted 19 September 1997

Age and Origin of the Moon

Der-Chuen Lee,* Alex N. Halliday, Gregory A. Snyder, Lawrence A. Taylor

The age and origin of the moon have been studied with the use of the recently developed short-lived hafnium-tungsten chronometer (^{182}Hf-^{182}W, half-life of nine million years). The tungsten isotopic compositions of 21 lunar samples range from chondritic to slightly radiogenic ($\varepsilon_W = -0.50 \pm 0.60$ to $+6.75 \pm 0.42$). This heterogeneity may have been inherited from material excavated from Earth and the putative impactor, but it is more likely the result of late radioactive decay within the moon itself; in this case, the moon formed 4.52 to 4.50 billion years ago, and its mantle has since remained poorly mixed.

The most widely accepted model for the origin of the moon is that during the later stages of Earth's accretion the impact of a colliding planet at least the size of Mars generated both the hot debris to form the moon and the angular momentum of the Earth-moon system (*1*, *2*). Yet, inconsistencies in this model persist (*3*, *4*). For example, it has long been argued on geochemical grounds that most of the material that formed the iron-depleted moon was derived from the silicate Earth after the formation of its core (*4*). This view is disputed by some (*5*), and others have argued, on the basis of their simulations, that the moon must have been derived largely from the mantle of the impactor (*2*, *6*). This latter view is considered by some to be inconsistent with the moon's many "Earth-like" features (*7*, *8*).

The ^{182}Hf-^{182}W [half-life = nine million years (m.y.)] chronometer can be used to investigate this problem. Because hafnium and tungsten are both highly refractory, planets and planetesimals that formed early in the history of the solar system should have relative proportions of these elements similar to those found in chondrites (*9*–*11*). However, Hf is lithophile (silicate-loving), whereas W is normally siderophile (metal-loving), such that core formation results in a dramatic intraplanetary fractionation of Hf and W. If this fractionation takes place during the lifetime of ^{182}Hf, the silicate reservoir, which has a high Hf/W ratio, will develop an excess abundance of ^{182}W relative to that found in chondritic bodies. Impacts

D.-C. Lee and A. N. Halliday are in the Department of Geological Sciences, University of Michigan, Ann Arbor, MI 48109–1063, USA. G. A. Snyder and L. A. Taylor are with the Planetary Geosciences Institute, Department of Geological Sciences, University of Tennessee, Knoxville, TN 37996, USA.

*To whom correspondence should be addressed. E-mail: dclee@umich.edu